Using very high resolution (VHR) imagery within a GEOBIA framework for gully mapping: an application to the Calhoun Critical Zone Observatory

A. Francipane, G. Cipolla, A. Maltese, G. La Loggia and L. V. Noto

ABSTRACT

Gully erosion is a form of accelerated erosion that may affect soil productivity, restrict land use, and lead to an increase of risk to infrastructure. An accurate mapping of these landforms can be difficult because of the presence of dense canopy and/or the wide spatial extent of some gullies. Even where possible, mapping of gullies through conventional field surveying can be an intensive and expensive activity. The recent widespread availability of very high resolution (VHR) imagery has led to a remarkable growth in the availability of terrain information, thus providing a basis for the development of new methodologies for analyzing Earth's surfaces. This work aims to develop a geographic object-based image analysis to detect and map gullies based on VHR imagery. A 1-meter resolution LIDAR DEM is used to identify gullies. The tool has been calibrated for two relatively large gullies surveyed in the Calhoun Critical Zone Observatory (CCZO) area in the southeastern United States. The developed procedure has been applied and tested on a greater area, corresponding to the Holcombe's Branch watershed within the CCZO. Results have been compared to previous works conducted over the same area, demonstrating the consistency of the developed procedure.

Key words | ecognition, GEOBIA, gully erosion, landforms analysis, soil erosion

A. Francipane (corresponding author)
G. Cipolla
A. Maltese
G. La Loggia
L. V. Noto
Dipartimento di Ingegneria (DI),
Università di Palermo,
Viale delle Scienze, 90142 Palermo,
Italy
E-mail: *antonio.francipane@unipa.it*

INTRODUCTION

Overland flow erosion can be considered as a threshold process occurring only after resistance forces are exceeded (Huggett 1990; Francipane *et al.* 2012). Entity and evolution of this phenomenon depends on several factors, such as the hydrological regime, the geomorphological characteristics, the climate, and the land use of the basin (Pimentel *et al.* 1995; Nearing *et al.* 1999; Wilkinson & McElroy 2007; Francipane *et al.* 2015). All of these factors are related to each other and determine, to a different degree, the extent of the erosive process, changes on soil productivity, landscape evolution, and its variations in space and time (Henderson-Sellers 1994; Kirkby & Cox 1995).

Erosion typically starts as a series of subparallel rills parallel to the slope gradient. Slight variations in surface topography can produce greater depth of flow, resulting in increased erosive forces and in an accelerated erosion, which promotes the evolution of rills into more severe forms of erosion: the gullies (Ritter *et al.* 2011). According to Poesen *et al.* (2003), the total soil losses caused by gully erosion could rise up to 90% in different parts of the world, restricting land use and increasing risk to infrastructure. For all of these reasons, gully erosion and their identification in the territory have always attracted the interest of the scientific community (Valentin *et al.* 2005).

The first attempts to study gullies go back to the 1930s, when Ireland *et al.* (1939) tried to study and describe the conditions governing the development of gullies in the Piedmont of South Carolina. In the 1960s, Tuckfield (1964) described the processes that led to the formation of gullies in the New Forest in Hampshire (England) and Seginer

doi: 10.2166/hydro.2019.083

(1966) presented different methods to quantify gully erosion. Patton & Schumm (1975) tried to describe the relationship between critical valley slope and drainage-basin area and use it as a predictive model to locate those areas of instability within alluvial valleys where gullies could form. In 1977, the Soil Conservation Service (SCS 1966) used a multivariate analysis to predict gully growth, while Stocking (1980) used multiple regression analysis to predict gully-head retreat on 66 gullies in Zimbabwe. Kirkby & Bracken (2009) made an interesting synthetic review of gully morphology and genesis examining the conditions for gully formation, focusing on gully initiation, head and side-wall processes, and making a brief dissertation about implications for gully prevention and remediation.

The advent of digital elevation models (DEMs) led to the birth and diffusion of quantitative land-surface analysis (i.e., geomorphometry) (Grosse *et al.* 2012). For many years, the main problem related to the use of DEMs for land-surface analysis has been their relatively low spatial resolution. The issue seems to be overcome with the advent of very high resolution (VHR) imagery, which started with the launch of IKONOS in 1999 and which finds nowadays its maximum expression in LIDAR data, that allow the derivation of very high resolution digital surface models (DSMs) and bare ground DEMs. These products, which constitute a basic support for activities such as hydrological–hydraulic modeling and the identification of areas exposed to flood risk, have provided the opportunity to develop new methodologies for analyzing Earth surfaces (Tarolli *et al.* 2009) that have found widespread use also in identifying the scars of gullies in the landscape in the last decade (Jackson *et al.* 1988; Ritchie *et al.* 1994; James *et al.* 2007; Noto *et al.* 2017; Francipane *et al.* 2018).

So far, today, there are mainly two different procedures to deal with high-resolution DEMs: a per-pixel approach (pixel-based) and a per-object approach (object-based). The last one is often referred to as object based image analysis (OBIA or GEOBIA if it takes into account the geographical aspect as well). While the pixel-based approach uses the classical rules of map algebra applied to the pixel, the object-based approach uses the concept of the image object, which is defined as a group of neighbor pixels with similar characteristics. The main advantage of such an approach is that object characteristics (e.g., mean value, standard deviation, ratio, etc.) and features (e.g., shape and texture) can be calculated and used to differentiate land cover classes with similar spectral information. These extra types of information give OBIA the potential to produce classifications characterized by accuracies higher than those produced by traditional pixel-based method.

One of the earlier efforts in detecting gullies by means of OBIA techniques was made about ten years ago by Eustace *et al.* (2009). The authors developed a semi-automated method to predict the presence and volume of gullies for unsampled locations within the Fitzroy catchment in the Great Barrier Reef lagoon, on the east coast of Australia. They used data from 20 LIDAR transects acquired in 2007. Shruthi *et al.* (2015) conducted a study with the aim of quantifying temporal changes in gully system areas applying the OBIA to a 1-meter resolution DEM obtained from the IKONOS mission. The authors were successful in achieving the gullies by developing a set of improved rules based on the knowledge of gully landform and process related to their formation. D'Oleire-Oltmanns *et al.* (2014) put together the GEOBIA analysis and the expert knowledge to set up an ensemble of rules to delineate gullies. They used as input a multispectral QuickBird 2 satellite image and calculated the accuracy by comparing the results of their classification with the reference data obtained by field surveys. Yang *et al.* (2017) developed and applied a multidirectional hill-shading method to extract gullies with an OBIA approach. The approach allowed the authors to get boundaries of gullies with high location accuracy and solve the discontinuity and low location accuracy caused by the pixel-based methods. Rahmati *et al.* (2017) submitted evidence that the GEOBIA technique is less expensive than any other approach to detect gullies, such as soil erosion measurements, especially over the last few years because it leads to the highest values of accuracy. In their paper, gully erosion mapping was performed using a DEM, a SPOT-5 panchromatic satellite image, and a multiresolution segmentation.

Starting from knowledge about morphology and geomorphological processes leading to gullies, this paper aims to develop a set of rules about morphometric aspects and processes related to the formation of these landforms for the identification of gullies within a GEOBIA framework. The framework is applied to the Calhoun Critical Zone

Observatory where several gullies have been observed and mapped by other studies (James *et al.* 2007; Noto *et al.* 2017) and where a very high resolution (i.e., 1 m) LIDAR DEM is available. The procedure, first calibrated for two gullies detected during a field survey carried out in June 2015, will be applied to the Holcombe's Branch watershed and results compared to those obtained by Noto *et al.* (2017). The framework has been developed within the software *eCognition developer 9.2* (Trimble Geospatial).

STUDY AREA AND DATASET: THE CALHOUN CRITICAL ZONE OBSERVATORY

The Calhoun Critical Zone Observatory (CCZO) is located in South Carolina (USA) and is part of the Critical Zone Observatory (CZO) project, which involves different institutions with the main goal to study and understand the processes that shape the surface of Earth and support terrestrial life.

The study site is on gentle slopes (<3%) that are covered by Appling and Cataula series soils (clayey, kaolinitic, thermic Typic Kanhapludults). These soils have a depth higher than 8 m to bedrock and are derived from granitoid gneiss, mica gneiss, and granite (Overstreet & Bell 1965). The soil has well-developed horizons with sandy loam in A and E horizons, clays in Bt horizons and deep saprolite C horizons (Fimmen *et al.* 2008). The upper 35-cm layer is coarse textured (68% sand, 15% clay), which ensures macroporosity to the soil (Richter *et al.* 1999). The groundwater depth is generally higher than 5 m, even though during winter and occasional summer rain events water can perch in the upper 1.5 m of the soil.

These soils supported crops of cotton, corn, and wheat during the 1800s through the first half of the 20th century, during which time, agricultural practices on Piedmont soils such as these included increased use of fertilizers and soil conservation practices (Sheridan 1979).

The CCZO is a particularly interesting site for studying gully erosion since after more than a century of intensive crop production, landscapes were abandoned and experienced severe erosion that has led to the loss of almost 20 cm of top soil with the formation of numerous gullies. Today, the gullies are mainly blanketed by reforestation, but the scars of these particular landforms are still present. More details about this area can be found in James *et al.* (2007).

Following the same work scheme of Noto *et al.* (2017), we identified a first area (SUBAREA-A) of about 1 km^2, containing two gullies surveyed during a field survey carried out in June 2015, and a second area (SUBAREA-B) with an extension of about 4.3 km^2, corresponding to the Holcombe's Branch watershed within the CCZO (Figure 1).

METHODS

The methodology builds on the use of four different morphometric indices able to detect the presence of specific landforms, which can be interpreted as part of a gully (bottom and edges): the Topographic Position Index (*TPI*), the terrain slope, the roughness slope, and the length to width ratio.

With reference to the data, LIDAR DEM was obtained by the study of Noto *et al.* (2017). The SUBAREA-A was used to develop and calibrate the GEOBIA procedure, while the SUBAREA-B was used to test the developed procedure. Figure 1 shows the LIDAR DEM for the SUBAREA-A (left part of the figure) and the SUBAREA-B (right part of the figure). Detailed information about the data and the two sub-areas can be found in Noto *et al.* (2017).

The following section is organized as follows. The section 'Morphometric indices' provides a brief description of the aforementioned indices. The section 'Gully detection within a GEOBIA framework' summarizes the OBIA procedure developed to identify gullies within the SUBAREA-A with particular reference to the two main phases of OBIA: segmentation and its calibration ('The *multiresolution segmentation* algorithm') and classification ('The object-based classification').

Morphometric indices

TPI for gully bottom

The *TPI* (Guisan *et al.* 1999; Jenness 2006) is defined as the difference between the elevation of a central pixel, z, and the mean elevation, $\bar{z}_\alpha$, of its surrounding cells within the kernel of size α. Negative values mean the cell is lower than its

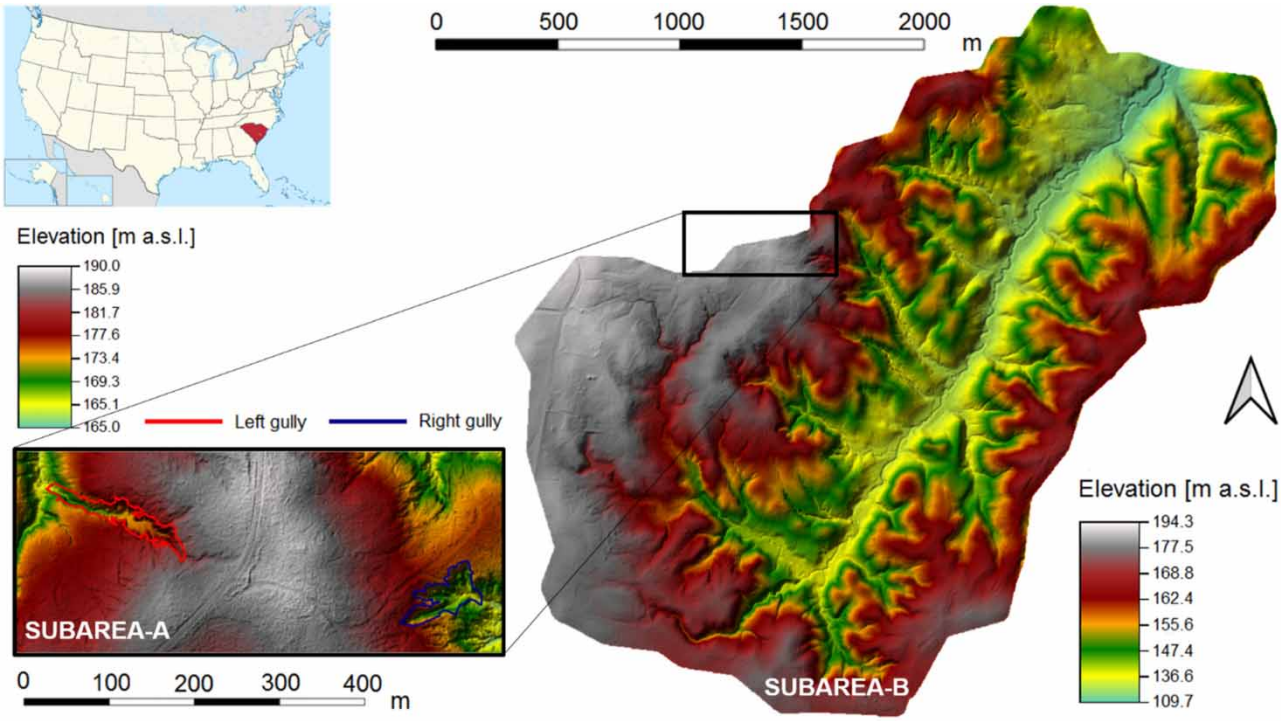

Figure 1 | LIDAR DEM of the SUBAREA-B (Holcombe's Branch watershed) of the CCZO (on the right) and focus on the SUBAREA-A (on the left) containing the two gullies surveyed and used for the calibration of the GEOBIA procedure.

surroundings. If z is significantly lower than $\bar{z}_\alpha$, which implies significant low values of *TPI*, then the cell is likely at or near the bottom of a depression (e.g., the bottom of a valley or a gully). In particular, we used the normalized *TPI* (*nTPI*) by dividing it by the mean value of elevation within the used kernel:

$$nTPI_\alpha = \frac{(z - \overline{z_\alpha})}{\overline{z_\alpha}} \quad (1)$$

Since the *TPI* is kernel-dependent, in order to decide the size of the kernel to use, we used different kernel size α (see 'Gully detection within a GEOBIA framework'). The $nTPI_\alpha$ was calculated in QGIS 3.4.0 (QGIS Development Team, http://qgis.org) starting from the existing GRASS *r.neighbors* function.

Terrain slope for gully edge

Terrain slope, which is the first spatial derivative of the terrain elevations, is one of the basic terrain parameters widely used in terrain analysis and landform classification. Slope has been here adopted as index of gully edge presence since the gully edges can be assimilated to abrupt changes of slope in the terrain (Shruthi *et al.* 2011; Liu *et al.* 2017). It was obtained in QGIS 3.4.0 from the LIDAR DEM through using the existing GRASS *r.slope.aspect* tool.

Terrain roughness for gully edge

Terrain roughness is a morphometric measure expressing irregularities of the soil surface, caused by factors such as soil texture, aggregate size, rock fragments, vegetation cover and land management. Since a DEM-derived roughness characterizes the local variance of surface gradients, distinguishing between smooth and rugged landforms might be a useful indicator of gully edge presence (Liu *et al.* 2017). According to Liu *et al.* (2017), here the terrain roughness is defined as the inverse of the cosine of slope angle and obtained using Equation (2) within the *raster calculator* of QGIS 3.4.0:

$$r = \frac{1}{\cos(slope)} \quad (2)$$

Since the roughness is directly derived from slope, in order to verify that the information provided by the terrain roughness is not redundant in detecting the edges of gullies, some tests for the SUBAREA-A have been carried out. The results of the tests, which are not shown here for the sake of brevity, demonstrated that considering this variable reduces the number of false positives, i.e., non-gully segments assigned to the class *gully edge*.

Length to width ratio for gully edge

Since gullies are usually narrow and long landforms, elements representing the edges are likely to have one of the two dimensions higher than the other one (Eustace *et al.* 2009; D'Oleire-Oltmanns *et al.* 2014). This information is contained within the length to width ratio, which gives an indication of the compactness of an element. In particular, values of length to width ratio greater than one means that the object is longer in one of its two dimensions. The index has been obtained in *eCognition developer 9.2*.

Gully detection within a GEOBIA framework

The gully detection procedure here developed can be summarized in the flow charts of Figure 2. The first step is the derivation of the first three aforementioned indices (*nTPI*, terrain slope, and terrain roughness). In particular, for the *nTPI* index, Evans & Lindsay (2010) suggest choosing the kernel size as a function of the typical width of the gullies to detect. In order to determine the best kernel size to detect gullies, *nTPI* was derived at three different kernel sizes, equal to 10, 20, and 30 m, respectively.

The second step consists of using the *nTPI* layer within *eCognition developer 9.2* as starting layer to apply the

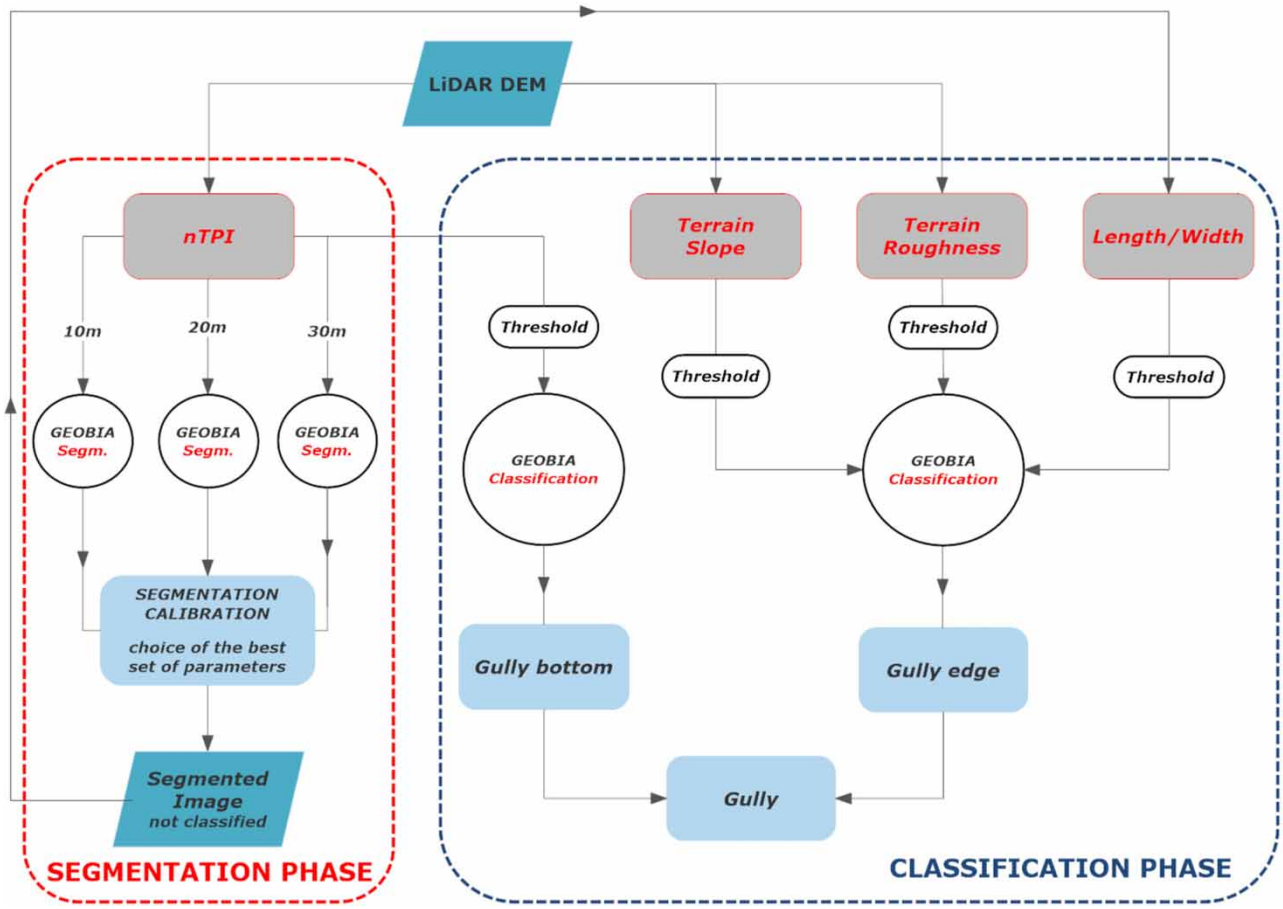

Figure 2 | Flow chart of proposed gully detection procedure.

segmentation process, which is the main process of *OBIA* (Hay & Castilla 2008), in order to derive homogeneous pixel clusters (also called segments or objects) that provide the base layer for the following analysis steps. Among the variety of segmentation algorithms, here it was decided to use the *multi-resolution segmentation* algorithm (Baatz & Schape 2000). It is a bottom-up approach that aims to merge neighbor pixels having a heterogeneity parameter less than a specific threshold, fixed by the user. Compared to the classical pixel-based approach, this process leads to a number of elements to process lower than that of pixels that make the original image and, for this reason, easier and faster to analyze. The optimal values of parameters, in order to obtain the segments from the original image, have been defined through a calibration procedure of segmentation detailed in the section 'The *multi-resolution segmentation* algorithm'.

A final phase of classification, based on different aspects of objects, such as spectral or textural attributes, allows the user to classify images and recognize a landform in the landscape (e.g., gullies in the present study). A *developed rulesets* section allows the user to set up an ensemble of rules aiming to automate the process and replicate it on different areas. A section called *Image Object Information* enables the user to query and get the values of some specific variables within an object and use them to set up a process tree of rules and/or algorithms aimed to detect a given object (e.g., gullies).

The *multi-resolution segmentation* algorithm

Segmentation creates segments or objects representing features that may be spectrally variable at the level of the single pixel. The most important parameter in order to identify homogeneous objects is the *scale parameter*, *e*, consisting of the maximum heterogeneity, or degree of fitting, between two neighbor pixels or objects. As the *scale parameter* increases, the number of merged pixels into a single object or the number of merged objects into a bigger object increases as well. On the contrary, as the *scale parameter* decreases, the original image will be fragmented into a higher number of small objects.

Actually, the similarity between two adjacent objects is evaluated as a function of a spatial and a spectral component (Happ *et al.* 2010). The first one depends on the spatial heterogeneity, h_{shape}, weighted by w_{shape}, and the compactness, h_{cmpct}, weighted by w_{cmpct}. For more details, see the first section of the Supplementary material, 'The *multi-resolution segmentation* algorithm'.

One way to optimize the values of the above parameters is to calibrate the segmentation procedure (Clinton *et al.* 2010; Liu *et al.* 2012, 2017). According to Liu *et al.* (2012), the overlay between the reference polygon (e.g., the actual gullies' boundaries) and the corresponding segments could generate under-segmented and over-segmented areas, apart from the overlapped areas (Figure 3). As is possible to see in Figure 3, the relationships between the reference polygons (continuous line in Figure 3) and the corresponding segments (dashed line in Figure 3) can be: one-to-many, one-to-one, and many-to-one.

According to the schemes depicted in Figure 3, it is possible to affirm that the goodness of the *multi-resolution segmentation* result, as far as concerning the geometric relationships, can be measured through the following three metrics:

$$OS = \frac{\sum |r_i - s_k|}{\sum |r_i|} \tag{3}$$

$$US = \frac{\sum |s_k - r_i|}{\sum |s_k|} \tag{4}$$

$$ED_1 = \sqrt{\frac{OS^2 + US^2}{2}} \tag{5}$$

In Equations (3) and (4), the term r_i stands for the reference polygon and the term s_k represents the segment that has to be compared with the reference polygon. In general, Equation (3) provides the *over-segmentation* factor (*OS*), because it sums up the areas included in the reference polygon but not in its corresponding segments. The output given by Equation (4) is the *under-segmentation* factor (*US*), since it is representative of all those pixels included in the segments, but that are outside the reference polygon. The output provided by Equation (5) is the *Euclidean distance* 1 (ED_1) and is the distance from the perfect geometric segmentation result. By analyzing Equations (3)–(5), it is easy to affirm that in the ideal case of perfect match between the reference polygon(s) and the segment(s) all the three metrics should be equal to zero. The over-segmentation

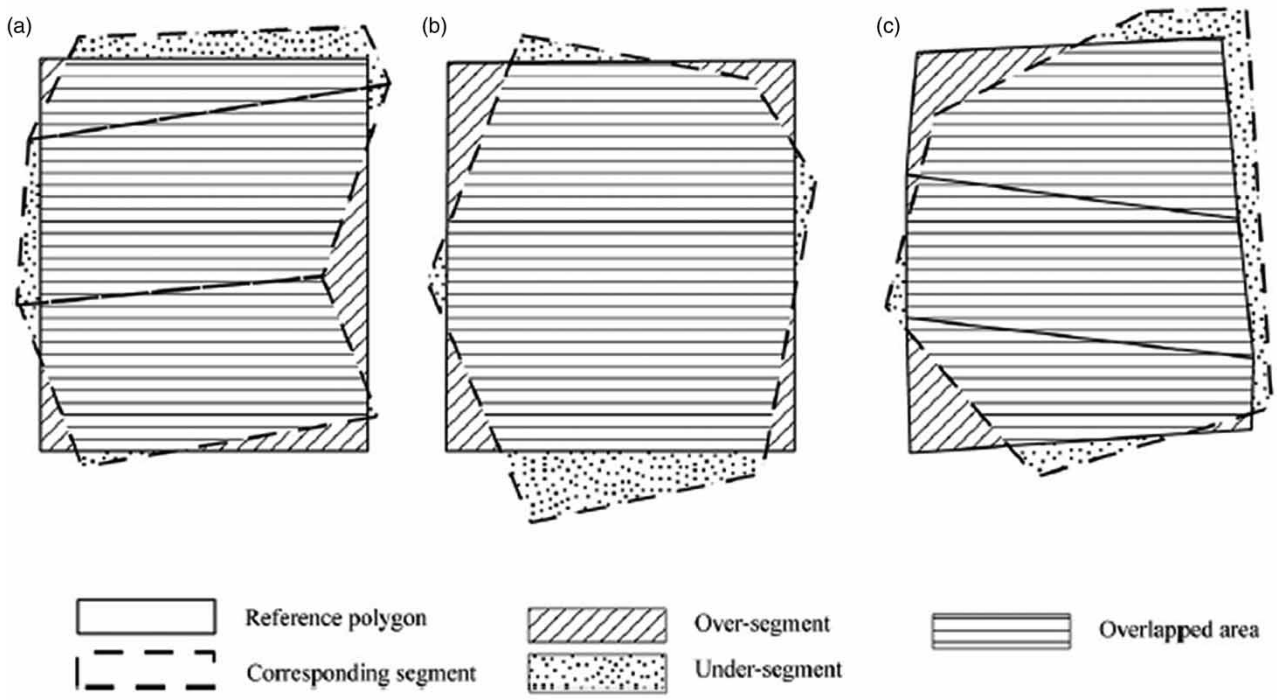

Figure 3 | Comparison between the reference polygon and the corresponding segments: (a) displays the one-to-many relationship, (b) the one-to-one, and (c) the many-to-one. Figure from Liu *et al.* (2012).

and the under-segmentation are two of the main limitations of object-based approach of images (Figure 3), which can affect the subsequent classification process in two ways: (i) under-segmentation results in image objects that cover more than one class and thus introduce classification errors because all pixels in each mixed image object have to be assigned to the same class; and (ii) features extracted from images affected by over-segmentation or under-segmentation do not represent the properties of real objects on the Earth such as shape and/or area (Liu & Xia 2010).

In order to take into account the arithmetic relationships as well, Liu *et al.* (2012) proposed the following new indices:

$$PSE = \frac{\sum |s_i - r_k|}{\sum |r_k|} \tag{6}$$

$$NSR = \frac{|m - v|}{m} \tag{7}$$

$$ED_2 = \sqrt{PSE^2 + NSR^2} \tag{8}$$

where *PSE* and *NSR* stand for *potential segmentation error* and *number of segment ratio*, respectively, while m and v represent the number of reference polygons and the number of corresponding segments, respectively. ED_2 is the *Euclidean distance* 2 and measures the distance from the perfect arithmetic segmentation.

In order to come up with a single index value that takes into account both the geometric and arithmetic segmentation results, the ED_1 and ED_2 have been combined into the key performance indicator, *KPI* (Goepel 2018), of Equation (9):

$$KPI = \sum_{i=1}^{k} w_i \cdot IC_i \tag{9}$$

where $k = 2$ (i.e., ED_1 and ED_2), w_i is the weight of IC_i, here assumed equal to 0.5 for both ED_1 and ED_2, and IC_i is calculated by means of Equation (10):

$$IC_i = 100 \cdot \frac{PI_i - base_i}{target_i - base_i} \tag{10}$$

where PI_i is the value of the i^{th} index (i.e., ED_1 and ED_2), $base_i$ is the value indicating the worst performance of

the i^{th} index and $target_i$ is the value indicating the best performance of the i^{th} index (i.e., zero for both ED_1 and ED_2). The *KPI* ranges between 0 and 100, with 100 indicating a perfect match in terms of geometric and arithmetic results.

More details about the multi-resolution algorithm can be found in the first section of the Supplementary material, 'The *multi-resolution segmentation* algorithm'.

The object-based classification

Object-based classification involves categorization of pixels on the basis of the spatial relationship with the neighboring pixels. Differently from the pixel-based classification, the object-based classification attempts to mimic what the human eyes do during visual interpretation based on the spectral properties (i.e., color), size, shape, and texture of objects obtained with the segmentation.

The process relies on the construction of one or more rules that can be used in cascade across a variety of layers to classify the segments resulting from the *multi-resolution segmentation* algorithm; such a procedure allows the user to produce a repeatable methodology. Depending on the purpose of the classification, it is possible to set different kinds of rules. As an example, some rules aim to classify objects on the basis of a threshold. In this case, the threshold value can be calibrated on the basis of literature indications or, in the absence of those, querying the values of some specific variables within objects falling within an interest area. Some other rules can be written up on the basis of adjacency or distance between segments.

The software *eCognition developer 9.2* allows the user to create different rules working with one or more layers, since they can be linked through logical *or* and *and* operators. Each rule can be independent from the others or linked to them in a cascade of rules, where each rule operates on the classified segments from the previous ones.

As it is possible to understand from the above considerations, a good classification requires a good a priori knowledge of the area and the types of land cover under investigation, which may not necessarily be available. Further, there is no definitive algorithm or parameters for the creation of image objects.

Method setup and calibration: application to the SUBAREA-A

Following the approach proposed by Clinton *et al.* (2010) and later applied by Liu *et al.* (2017) to identify gullies in the Yaojiawan catchment (Shaanxi Province, China), the proposed method has been previously calibrated on the two surveyed gullies of SUBAREA-A shown in Figure 1. Such an optimization process is very convenient, since it enables to compute segments fitting the actual boundaries of the two considered gullies in the most proper way.

The proposed methodology involves making choices of many different parameters, which may influence the resulting outcome in terms of accuracy of the identification of gullies. Main choices regard the *nTPI* kernel, α, and the segmentation parameters (i.e., e, w_{shape}, and w_{cmpct}). With reference to the *nTPI*, three different kernel sizes (i.e., 10, 20, and 30 m) were fixed a priori on the basis of a simple qualitative visual analysis and considering that the two gullies of the SUBAREA-A both have a width of about 20 m. With reference to the segmentation parameters, instead, a certain range of variability for the *scale parameter* (i.e., 3, 5, 10, and 20) and the weights related to the spatial heterogeneity and the compactness factor has been explored. In more detail, w_{cmpct} has been set equal to 0.2, 0.45, and 0.9, while w_{shape} is equal to 0.2, 0.6, and 0.9.

The *KPI* (see the section 'The *multi-resolution segmentation* algorithm') has been used to obtain the set of parameters that provides the best segmentation and the confusion matrix to evaluate the goodness of the final classification.

Multi-resolution segmentation

Based on morphology and the most common shape of gullies, the expected result of segmentation should have thin and long segments corresponding to the gully-affected areas and more compact segments outside them. Considering what was said in the section 'The *multi-resolution segmentation* algorithm', once the *scale parameter*, e, is fixed, these results should be obtained for low weights of the spatial heterogeneity and compactness factor.

In order to perform the *multi-resolution segmentation* algorithm, the only layer of the *nTPI* has been used.

In order to calibrate the process, a number of 108 possible combinations resulting from the considered ranges of variability of *nTPI* (3), e (4), w_{shape} (3), and w_{cmpct} (3) have been considered by setting up an ensemble of segmentation attempts and evaluating, for each of them, the goodness of the results in terms of *KPI*. The results of calibration, not shown here for the sake of brevity, demonstrated that the more suitable size for the kernel of the *nTPI* was 30 m (hereafter *nTPI*30). With reference to the two gullies of SUBAREA-A, a visual inspection of *nTPI*30 layer seems to ensure that pixels belonging to the gully-affected areas, either bottom or edges, and to the gully not-affected areas are likely to be included in the same kernel. In terms of *multi-resolution segmentation*, this means that all the pixels covering the bottom of a gully are likely merged into objects with strongly negative values of *nTPI*30; similarly, the edges of gullies are merged into objects still having negative values of *nTPI*30 but closer to zero than the object representing the bottom. More details about the 36 possible combinations and their results in terms of KPI can be found in the second section of the Supplementary material, 'Multi-resolution segmentation in SUBAREA-A'.

Figure 4(a) and 4(b) show the results of segmentation corresponding to the two surveyed gullies of SUBAREA-A relatively to $e = 10$, $w_{shape} = 0.9$, and $w_{cmpct} = 0.2$, while Figure 4(c) and 4(d) show the results of segmentation for

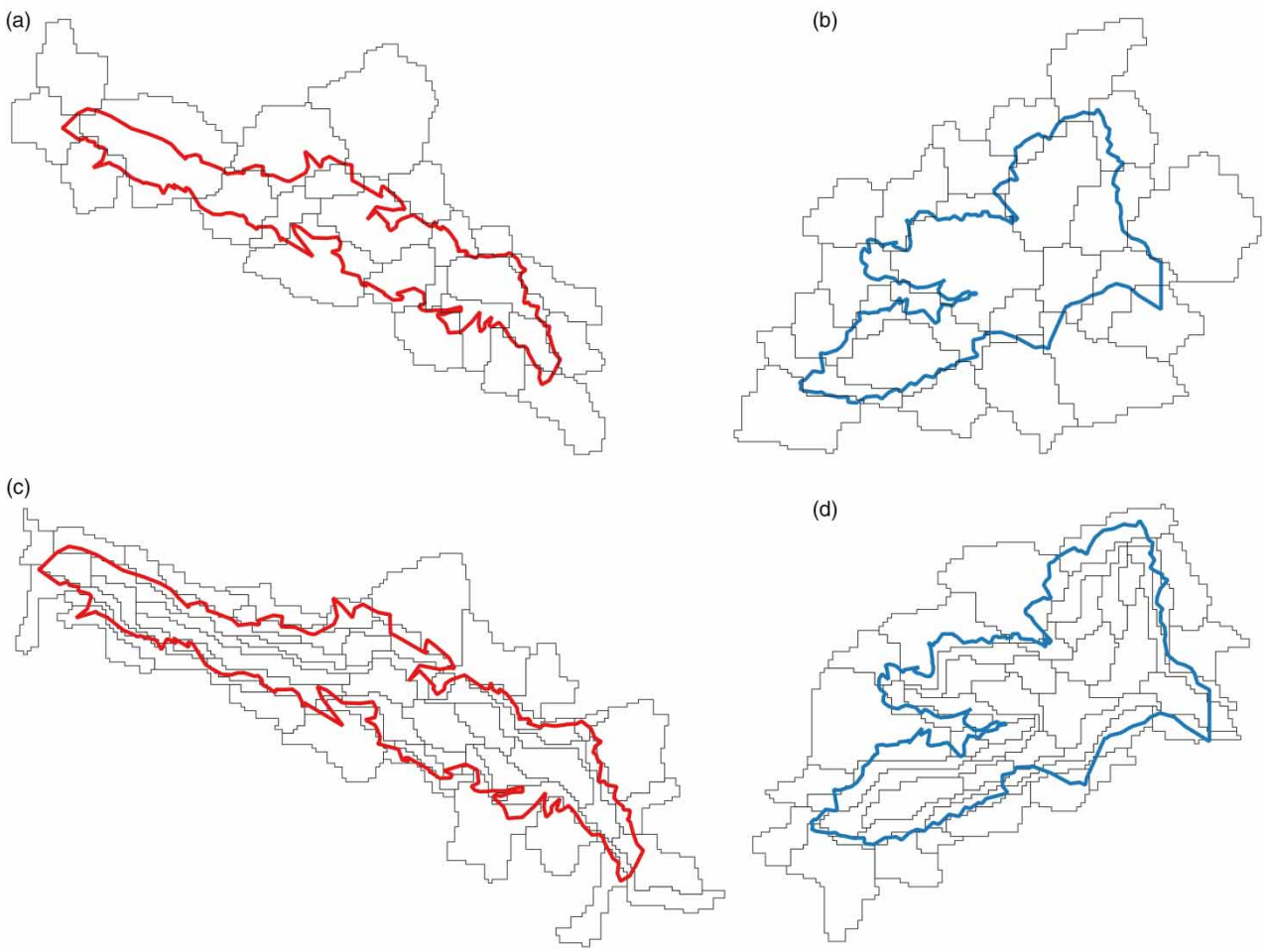

Figure 4 | Segmentation results for $e = 10$, $w_{shape} = 0.9$, and $w_{cmpct} = 0.2$ for the (a) left basin and (b) right basin and $e = 5$, $w_{shape} = w_{cmpct} = 0.2$ for the (c) left basin and (d) right basin. Black lines indicate segmentation.

$e = 5$, $w_{shape} = 0.2$, and $w_{cmpct} = 0.2$. The image segments displayed in Figure 4 are only those intersecting the actual gully-affected areas.

It is possible to notice in Figure 4 that, as the *scale parameter* increases, the size of objects increases as well. Looking at Figure 4(a) and 4(b) ($e = 10$), segmentations resulted in a low number of large objects leading to high values of *OS* and/or *US* and, consequently, higher values of ED_1. More importantly, there is a coarse segmentation inside the actual gullies that could result in a raw classification. The opposite considerations can be made by observing Figure 4(c) and 4(d), where e = 5. In this case, a higher number of long and narrow objects allows for a better description of geometry but a worse segmentation in terms of arithmetic results.

Considering the previous arguments, according to Baatz & Schape (2000), it has been decided to select the following values for the segmentation of SUBAREA-A: $e = 5$, $w_{shape} = w_{cmpct} = 0.2$.

Starting from this segmentation it has been possible to retrieve different information at the segment scale, among which is the length to width ratio, useful for the next step of classification.

Classification

Figure 5 shows the two surveyed gullies of SUBAREA-A overlaid to the spatial distributions of the four indices above mentioned: *nTPI*30 (Figure 5(a)), terrain slope (Figure 5(b)), terrain roughness (Figure 5(c)), and length to width ratio (Figure 5(d)). Looking at Figure 5(a), as already discussed in the section 'Multi-resolution segmentation', it is possible to notice that the objects belonging to the bottom of gullies are characterized by negative values, while edges are identified by still negative values but closer to zero. By observing the slope and the terrain roughness, shown in Figure 5(b) and 5(c), respectively, it is clear that the higher values of both these variables correspond to gullies' edges.

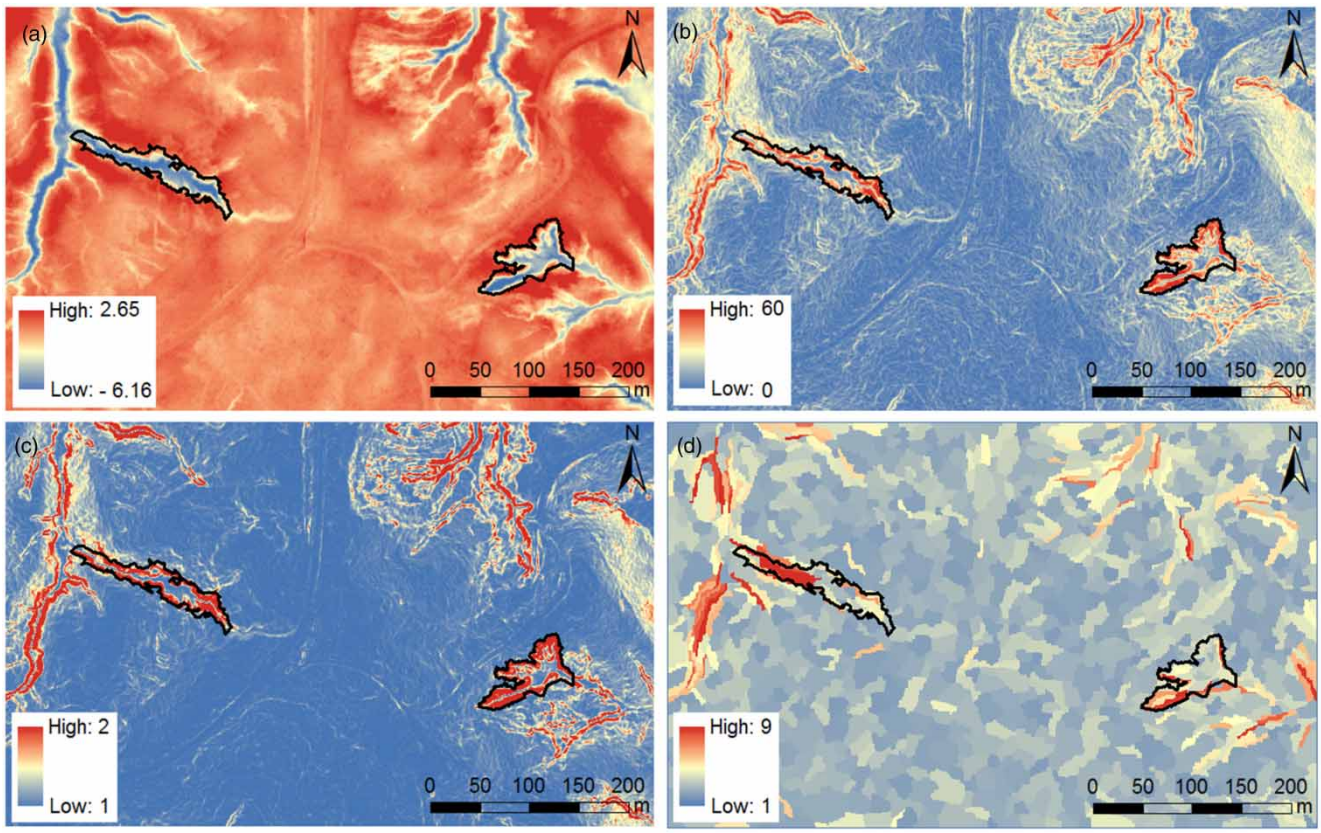

Figure 5 | Spatial distribution of the four indices used to detect gully bottom and edges: (a) TPI30, (b) slope, (c) terrain roughness, and (d) length to width ratio.

Finally, from Figure 5(d), it is possible to see that if the element is narrow and long, as gullies usually are, there are high values of length to width ratio.

Starting from information contained within the segmented objects that, differently from the classical pixel-based approach, can concern also the values of min, max, mean, standard deviation, etc., of a given variable, we tried to detect landforms connected to gullies. Investigation of previous layers allowed us to set up an ensemble of rules and algorithms to detect the bottoms and the edges of the two surveyed gullies of SUBAREA-A.

First of all, we identified the bottom of gullies by using the *nTPI* layer. As already said in the section '*TPI* for gully bottom', low values of *TPI* indicate a cell at or near the bottom of a valley that is likened to the bottom of a gully. That being said, by querying the mean value of *nTPI*30 for both those segments within and outside the surveyed gullies, it was possible to identify and calibrate the value of a threshold, T_1, distinguishing between the bottom and other landforms.

Once the bottom part of gullies within the SUBAREA-A was identified, for the identification of edges, a similar process led to the identification of three thresholds (i.e., T_2, T_3, and T_4) for the terrain slope, terrain roughness, and length to width ratio layers, respectively.

This process resulted in the writing of Equation (11), which is the first rule of the cascade process, for the identification of the bottom, and Equation (12) for the identification of edges:

$$Mean\ (nTPI30) < T_1 \tag{11}$$

$$\begin{cases} Mean\ slope > T_2 \\ Mean\ roughness > T_3 \\ Length/width > T_4 \end{cases} \tag{12}$$

Equation (11) affirms that, for each segment, if the average *nTPI*30 within the object is less than T_1 it is classified as a gully bottom. Equation (12) puts three different conditions together through an *and* spatial operator and, therefore, it represents an intersection. For this reason, only those objects where all of the three conditions are contemporarily satisfied are classified as gully edges. In particular, from previous analysis, the values of T_1, T_2, T_3, and T_4 resulted as equal to -2, 20°, 1.15, and 1.5, respectively.

All the segments classified as bottom or edges have been merged into a single class labeled *gully*, while all the unclassified objects have been assigned to a class labeled *non-gully*. The boundaries of the two surveyed gullies, highlighted in a continuous black line, overlaid to the classification results, are shown in Figure 6.

In order to verify the goodness of the achieved classification, the *Accuracy Assessment* tool provided by *eCognition developer 9.2* has been used for the same two rectangular frames surrounding the two gullies of SUBAREA-A retrieved by Noto *et al.* (2017) (see Box-SX and Box-DX, Figure 2a of Noto *et al.* (2017)). The tool returns the *overall*, the *user*, and the *producer accuracies* for the classes *gully* and *non-gully* and the *K-index* for both the two classes and takes into account all of the pixels contained in an object. In particular, the overall accuracy is the percentage of pixels correctly classified over the total number of them in the confusion matrix.

Since the overall accuracy is very satisfactory (almost 95% for the left gully and 91% for the right gully), in order to test the procedure developed for the SUBAREA-A, the same rules here discussed have been applied to detect gullies in the SUBAREA-B. More details about the *Accuracy Assessment* tool and its application to SUBAREA-A can be found in the third section of the Supplementary material, 'Classification in SUBAREA-A' and Table S1.

Application of the developed procedure to the SUBAREA-B

As was said in the section 'Classification', since the accuracy assessment related to the SUBAREA-A is satisfied, the same classification rules have been applied to detect the gullies within the SUBAREA-B. Because of the greater extension and the more complex morphology of the SUBAREA-B, as compared to the SUBAREA-A, in addition to the developed rules for the SUBAREA-A, other rules have to be used in order to exclude some morphological features (e.g., some parts of hydrological network and the bank erosion areas) which, at the watershed scale, can be erroneously classified as gullies.

In particular, for the correction of those objects belonging to the hydrological network, all of those objects with a mean value of flow accumulation lower than a threshold,

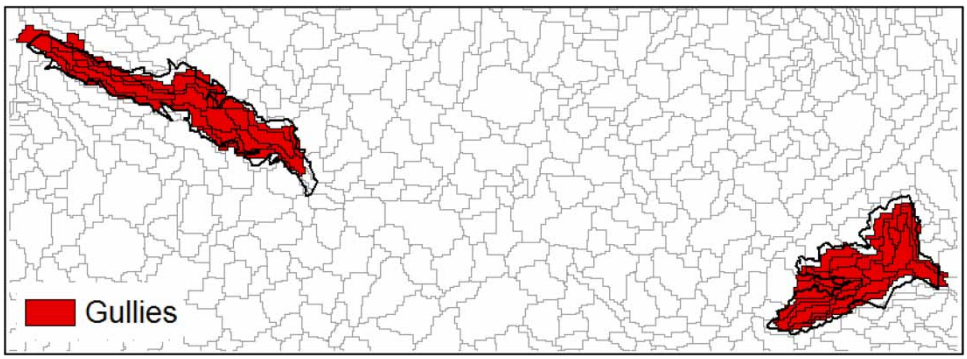

Figure 6 | Results of the classification procedure for the SUBAREA-A after applying Equations (11) and (12).

T_5, have been corrected as *non-gully*. The layer of flow accumulation for the Holcombe's Branch watershed was previously derived from the DEM in QGIS. For the correction of those objects belonging to the bank erosion areas, instead, we used a distance threshold, T_6, from those elements corrected as hydrological network at the previous step. In this case, all of those segments with a distance from the hydrological network lower than T_6 have been corrected as *non-gully*. This process resulted in the implementation of two new rules in *eCognition developer 9.2*:

$$Mean\ (Flow\ Accumulation) > T_5 \quad (13)$$

$$Distance\ to\ hydrological\ network < T_6 \quad (14)$$

In particular, investigation of objects belonging to the river network and to the bank erosion areas led to set $T_5 equal\ to$ 4, 000 *pxl* and $T_6 equal\ to$ 30 *pxl*.

In this case, since a spatial distribution of the digitalized actual gullies is not available, in order to assess the appropriateness of the developed procedure, the spatial map of results for the object-based procedure and the pixel-based procedure, developed for the same area by Noto *et al.* (2017), has been compared (Figure 7).

From an overview of Figure 7, it is possible to notice that the number of gullies detected with the object-based approach is higher than that obtained with the pixel-based approach. Moreover, while in some cases there is almost a perfect match between the gullies detected with the two approaches (see box B in Figure 7), in some other cases the match is only partial (see box A in Figure 7) and in some others there is not a match at all (see box C in Figure 7). Rarely, the pixel-based approach detects gullies that the object-based approach is not able to identify. However, observing the morphology of the Holcombe's Branch watershed in Figure 7, it seems plausible that the landforms identified by the object-based approach are likely gullies and there is a failure in identifying correctly these landforms from the pixel-based approach.

Starting from the distribution map of the gullies in Figure 7 we derived some indices of the gullies such as the area, the boundary length (i.e., perimeter), and the compactness index, and their empirical distribution function (*ecdf*, Figure 8). According to Noto *et al.* (2017), the compactness index was defined as the ratio between the perimeter of the gully and the root square of its area (multiplied by 4π). It ranges between 1.28 (most compact gully) and 5.31 (very elongated gully) and characterizes the shape of the extracted gullies; the more it is close to 1, the more the shape of the gully is close to a circle.

A total number of 143 gullies were identified with an area ranging between 20 m^2 and about 10,700 m^2 (Figure 8(a)), whereas the perimeter ranges from 24 m to about 1,950 m (Figure 8(b)). The compactness index (Figure 8(c)) ranges from a minimum of 0.04 (very elongated gullies) to a maximum of about 0.6 (more compact gullies). In order to compare the results of this study with the results of the pixel-based approach provided by Noto *et al.* (2017), Figure 8 shows also the *ecdf* for the area, perimeter, and compactness index returned by that study. As it is possible to notice from Figure 8, apart for the compactness index, which is perfectly overlapped to that of Noto *et al.* (2017), the object-based approach led to

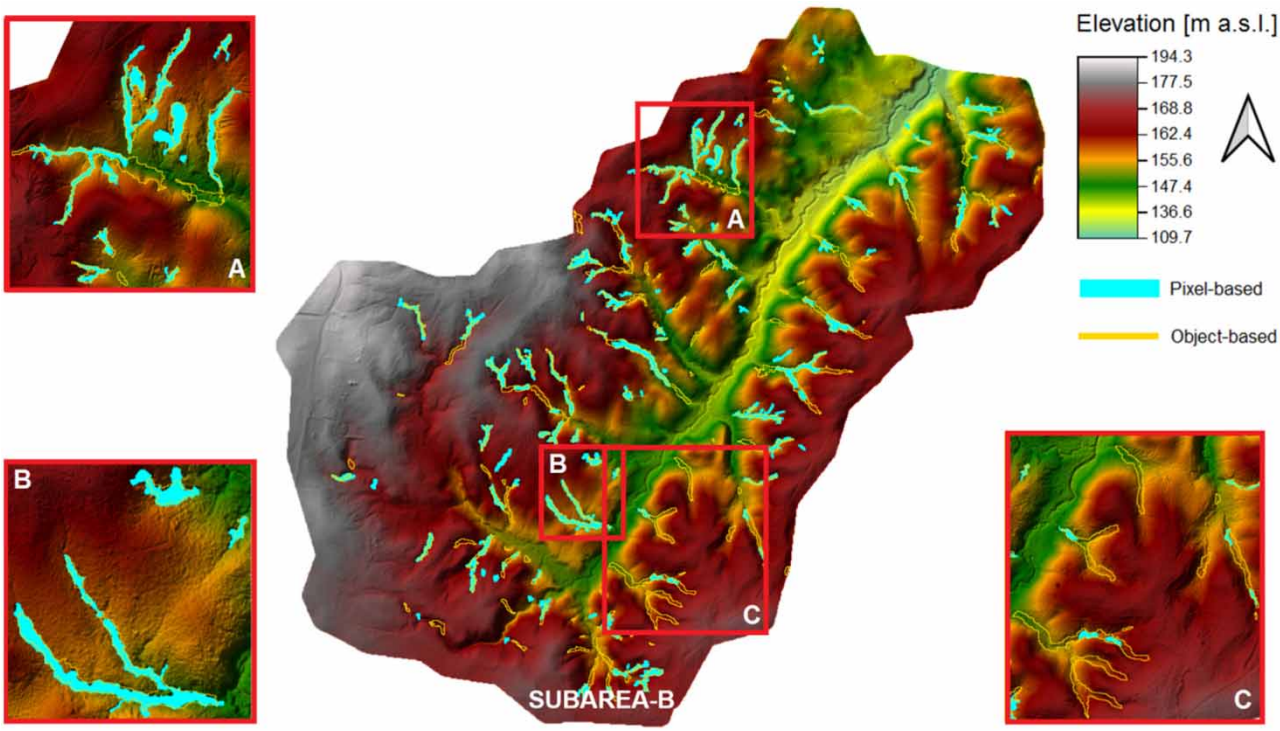

Figure 7 | Comparison between the gullies achieved through a GEOBIA technique and a pixel-based image analysis. Boxes A, B, and C show some focuses on the Holcombe's Branch watershed.

identifying more extended gullies (e.g., larger area and perimeter) than the pixel-based approach. While the difference in terms of upper limits is due to the two different approaches and, mainly, to the fact that the object-based approach works with elements, which are aggregation of pixels, where the minimum size of the element is not that of the pixel anymore, the different lower limit is mainly due to the fact that, differently from Noto *et al.* (2017), we did not eliminate from classification those gullies with an area smaller than a given threshold.

Some more statistical characteristics of extracted gullies can be found in the fourth section of the Supplementary material, 'Application of the developed procedure to the SUBAREA-B' and Table S2.

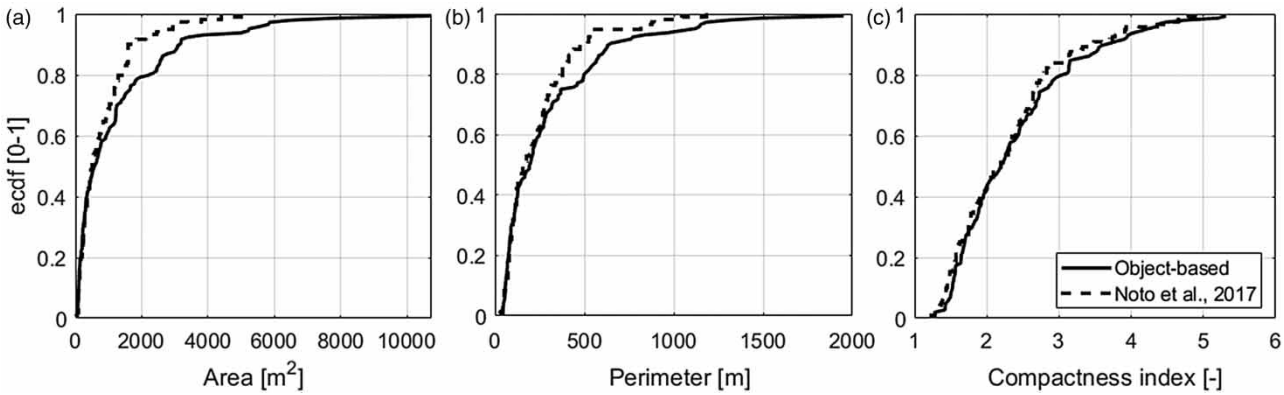

Figure 8 | Empirical cumulative distribution function (*ecdf*) of morphometric characteristics of gullies identified by the proposed methodology over SUBAREA-B: (a) area, (b) perimeter, and (c) compactness index.

DISCUSSION

Spatial distribution of gullies identified by the object-based approach here developed for the Holcombe's Branch watershed (Figure 7) seems to provide a good definition of the spatial pattern of gullies. The application of the procedure to SUBAREA-B provided the identification of gullies on the basis of segmentation and classification previously developed, calibrated, and tested for the SUBAREA-A. Differently than Noto *et al.* (2017), which removed the main river channel and the bank erosion landforms in the SUBAREA-B manually or by means of a threshold for the gullies' area, here we used a couple of rules related to the contributing area and to the distance from the channels, respectively.

In order to minimize the errors due to the over-segmentation and under-segmentation of images (Figure 3), some geometric and arithmetic relationships have been used to calibrate the segmentation on the SUBAREA-A. While the geometric relationship ensures the best match possible in terms of area and shape, the arithmetic relationship ensures the best segmentation in terms of number of objects (i.e., as few objects as possible). The geometric and arithmetic relationships have been combined in a unique index representative of the goodness of segmentation.

For the classification of objects, a set of rules based on parameters' thresholds and/or adjacency or distance from other objects has been used. Since a gully can be usually characterized by a bottom and some edges, which are defined by different characteristics, it has been preferred to set up a rule for the identification of the bottom and three rules in cascade for the identification of the edges. For the first case, we used the *nTPI*30 parameter, while for the edges we used the terrain slope, the terrain roughness, and the length to width ratio.

For the SUBAREA-B, the physical consistency of the developed procedure has been evaluated by comparing the gullies' pattern provided by the proposed method with that of Noto *et al.* (2017). From the observation of the Holcombe's Branch watershed morphology (Figure 7), the GEOBIA procedure seems able to detect also gullies, or parts of those, that have not been detected by the pixel-based approach. For this reason, it is plausible to say that the developed procedure is a reliable tool to identify gullies once it has been calibrated and tested. Moreover, the comparison of *ecdf* for some characteristics of the gullies such as the area, the perimeter, and the compactness index (Figure 8) showed that the object-based procedure leads to gullies with bigger ranges of area and perimeter than those identified by Noto *et al.* (2017).

One of the most important advantages of the proposed method consists of the reproducibility of the developed procedure also for other areas of the Earth. In contrast, the main limitation is the fact that parameters need to be recalibrated in order to adapt to different gully patterns.

CONCLUSIONS

An object-based approach to detect landforms is presented in this study. The approach, differently from the classical pixel-based approach, uses the characteristics and features of groups of pixels, called objects or segments, to differentiate land cover classes with similar spectral information. As compared to the pixel-based approach, the possibility to consider this extra information gives GEOBIA the potential to produce land cover thematic maps with a higher accuracy.

GEOBIA has been applied to the Calhoun Critical Zone Observatory (CCZO), an area of South Carolina particularly interesting since it is characterized by the presence of numerous gullies because of very intense erosion activity due to the abandonment of terrains used for intensive crop production in the past century.

The software used to carry out the study is the *eCognition developer 9.2*, developed by Trimble Navigation Ltd, which provides a collection of tools for OBIA and GEOBIA, facilitating the classification of images in various application fields. The software allows the user to develop a procedure that starts from the segmentation of an image to create groups of homogeneous pixels (also called objects or segments) to which is assigned the same class during the following classification process. The main advantage of the developed procedure, as compared to a classical pixel-based approach, is that the number of elements to process is significantly lower than that of pixels that make the image and, for this reason, easier and faster to analyze.

Two areas, the SUBAREA-A and the SUBAREA-B, inside the CCZO have been used to calibrate and test,

respectively, the developed procedure. The first area is characterized by the presence of two gullies detected during a field survey in June 2015. The surveyed gullies have been used as reference to calibrate the GEOBIA procedure and thus obtain the optimal segmentation and classification. The procedure, then, has been applied to the SUBAREA-B, corresponding to the Holcombe's Branch watershed, to test the goodness of the developed procedure.

Results showed that the GEOBIA procedure developed in *eCognition developer 9.2* is able to detect gullies with good accuracy even though, because of the absence of surveyed gullies for the SUBAREA-B, the results have been evaluated using as reference the results from a pixel-based approach developed for the same area by Noto *et al.* (2017).

Although the approach surely requires further testing in other gullied systems where good quality topographic data are available, the demonstrated capability of *eCognition developer 9.2* in developing OBIA or GEOBIA procedures to identify gullies in a given area of Earth, coupled with the increasing availability of LIDAR data, allows us to say that this automated technique has the potential for individuation of different landforms (e.g., landslides) and applications across a range of environments.

SUPPLEMENTARY MATERIAL

The Supplementary Material for this paper is available online at https://dx.doi.org/10.2166/hydro.2019.083.

REFERENCES

Baatz, M. & Schape, A. 2000 Multiresolution segmentation: an optimization approach for high quality multi-scale image segmentation. In: *Angewandte Geographische Informations-Verarbeitung, XII* (J. Strobl, T. Blaschke & G. Griesbner, eds). Wichmann Verlag, Karlsruhe, Germany, pp. 12–23.

Clinton, N., Holt, A., Scarborough, J., Yan, L. & Gong, P. 2010 Accuracy assessment measures for object-based image segmentation goodness. *Photogrammetric Engineering and Remote Sensing* **76**, 289–299.

D'Oleire-Oltmanns, S., Marzolff, I., Tiede, D. & Blaschke, T. 2014 Detection of gully-affected areas by applying object-based image analysis (OBIA) in the region of Taroudannt, Morocco. *Remote Sensing* **6**, 8287–8309.

Eustace, A., Pringle, M. & Witte, C. 2009 Give me the dirt: detection of gully extent and volume using high-resolution Lidar. In: *Innovations in Remote Sensing and Photogrammetry* (S. Jones & K. Reinke, eds). Springer, Berlin, Heidelberg, pp. 255–269.

Evans, M. & Lindsay, J. 2010 High resolution quantification of gully erosion in upland peatlands at the landscape scale. *Earth Surface Processes and Landforms* **35**, 876–886.

Fimmen, R. L., Richter, D. D., Vasudevan, D., Williams, M. A. & West, L. T. 2008 Rhizogenic Fe–C redox cycling: a hypothetical biogeochemical mechanism that drives crustal weathering in upland soils. *Biogeochemistry* **87**, 127–141.

Francipane, A., Ivanov, V. Y., Noto, L. V., Istanbulluoglu, E., Arnone, E. & Bras, R. L. 2012 TRIBS-Erosion: A parsimonious physically-based model for studying catchment hydro-geomorphic response. *Catena* **92**, 216–231.

Francipane, A., Fatichi, S., Ivanov, V. Y. & Noto, L. V. 2015 Stochastic assessment of climate impacts on hydrology and geomorphology of semiarid headwater basins using a physically based model. *Journal of Geophysical Research F: Earth Surface* **120**, 507–533.

Francipane, A., Mussomè, F., Cipolla, G. & Noto, L. V. 2018 Object-based image analysis technique for gully mapping using topographic data at very high resolution (VHR). In: *HIC 2018. 13th International Conference on Hydroinformatics* (G. La Loggia, G. Freni, V. Puleo & M. De Marchis, eds). EasyChair, Manchester, pp. 725–730.

Goepel, K. 2018 Implementation of an online software tool for the analytic hierarchy process (AHP-OS). *International Journal of the Analytic Hierarchy Process* **10**, 469–487.

Grosse, P., van Wyk de Vries, B., Euillades, P., Kervyn, M. & Petrinovic, I. 2012 Systematic morphometric characterization of volcanic edifices using digital elevation models. *Geomorphology* **136**, 114–131.

Guisan, A., Weiss, S. B. & Weiss, A. D. 1999 GLM versus CCA spatial modeling of plant species distribution. *Plant Ecology* **143**, 107–122.

Happ, P. N., Ferreira, R. d. S., Bentes, C., Costa, G. A. O. P. & Feitosa, R. Q. 2010 Multiresolution segmentation: a parallel approach for high resolution image segmentation in multicore architectures. In: *International Conference on Geographic Object-Based Image Analysis (GEOBIA 2010)*, Ghent, Belgium.

Hay, G. J. & Castilla, G. 2008 Geographic Object-Based Image Analysis (GEOBIA): A new name for a new discipline. In: *Object-Based Image Analysis: Spatial Concepts for Knowledge-Driven Remote Sensing Applications* (T. Blaschke, S. Lang & G. J. Hay eds). Springer, Berlin, Heidelberg, pp. 75–89.

Henderson-Sellers, A. 1994 Land-use change and climate. *Land Degradation & Development* **5**, 107–126.

Huggett, R. 1990 Book review. In: *Modelling Geomorphological Systems*, Vol. 15 (M. G. Anderson, ed.). Earth Surface Processes and Landforms, Chichester, pp. 292–293.

Ireland, H. A., Eargle, D. H. & Sharpe, C. F. S. 1939 *Principles of Gully Erosion in the Piedmont of South Carolina*. US Department of Agriculture, Washington, DC, USA.

Jackson, T. J., Ritchie, J. C., White, J. & Leschack, L. 1988 Airborne laser profile data for measuring ephemeral gully erosion. *Photogrammetric Engineering & Remote Sensing* **54**, 1181–1185.

James, L. A., Watson, D. G. & Hansen, W. F. 2007 Using LiDAR data to map gullies and headwater streams under forest canopy: South Carolina, USA. *Catena* **71**, 132–144.

Jenness, J. 2006 *Topographic Position Index (tpi_jen.avx) Extension for ArcView 3.x, v. 1.2, 1.2 ed*. Jenness Enterprises, Flagstaff, AZ, USA.

Kirkby, M. J. & Bracken, L. J. 2009 Gully processes and gully dynamics. *Earth Surface Processes and Landforms* **34**, 1841–1851.

Kirkby, M. J. & Cox, N. J. 1995 A climatic index for soil erosion potential (CSEP) including seasonal and vegetation factors. *Catena* **25**, 333–352.

Liu, D. & Xia, F. 2010 Assessing object-based classification: advantages and limitations. *Remote Sensing Letters* **1**, 187–194.

Liu, Y., Bian, L., Meng, Y., Wang, H., Zhang, S., Yang, Y., Shao, X. & Wang, B. 2012 Discrepancy measures for selecting optimal combination of parameter values in object-based image analysis. *ISPRS Journal of Photogrammetry and Remote Sensing* **68**, 144–156.

Liu, K., Ding, H., Tang, G., Zhu, A. X., Yang, X., Jiang, S. & Cao, J. 2017 An object-based approach for two-level gully feature mapping using high-resolution DEM and imagery: a case study on hilly loess plateau region. *China. Chinese Geographical Science* **27**, 415–430.

Nearing, M. A., Simanton, J. R., Norton, L. D., Bulygin, S. J. & Stone, J. 1999 Soil erosion by surface water flow on a stony, semiarid hillslope. *Earth Surface Processes and Landforms* **24**, 677–686.

Noto, L. V., Bastola, S., Dialynas, Y. G., Arnone, E. & Bras, R. L. 2017 Integration of fuzzy logic and image analysis for the detection of gullies in the Calhoun Critical Zone Observatory using airborne LiDAR data. *ISPRS Journal of Photogrammetry and Remote Sensing* **126**, 209–224.

Overstreet, W. C. & Bell, H. 1965 *The Crystalline Rocks of South Carolina: Relation of Rock Units in the Geologic Belts of the Piedmont and Blue Ridge Provinces of South Carolina*. Bulletin 1183, US Government Printing Office, Washington, DC, USA.

Patton, P. C. & Schumm, S. A. 1975 Gully erosion, northwestern Colorado: a threshold phenomenon. *Geology* **3**, 88–90.

Pimentel, D., Harvey, C., Resosudarmo, P., Sinclair, K., Kurz, D., McNair, M., Crist, S., Shpritz, L., Fitton, L., Saffouri, R. & Blair, R. 1995 Environmental and economic costs of soil erosion and conservation benefits. *Science* **267**, 1117–1123.

Poesen, J., Nachtergaele, J., Verstraeten, G. & Valentin, C. 2003 Gully erosion and environmental change: importance and research needs. *Catena* **50**, 91–133.

Rahmati, O., Tahmasebipour, N., Haghizadeh, A., Pourghasemi, H. R. & Feizizadeh, B. 2017 Evaluating the influence of geo-environmental factors on gully erosion in a semi-arid region of Iran: an integrated framework. *Science of the Total Environment* **579**, 913–927.

Richter, D., Markewitz, D., Trumbore, S. G. & Wells, C. 1999 Rapid accumulation and turnover of soil carbon in a re-establishing forest. *Nature* **400**, 56–58.

Ritchie, J. C., Grissinger, E. H., Murphey, J. B. & Garbrecht, J. D. 1994 Measuring channel and gully cross-sections with an airborne laser altimeter. *Hydrological Processes* **8**, 237–243.

Ritter, D. F., Kochel, R. C. & Miller, J. R. 2011 *Process Geomorphology*, 5th edn. Waveland Press, Long Grove, IL, USA.

SCS 1966 Procedure for determining rates of land damage, land depreciation and volume of sediment produced by gully erosion. US Dept. of Agriculture, Soil Conservation Service, Engineering Division, Washington, 1966.

Seginer, I. 1966 Gully development and sediment yield. *Journal of Hydrology* **4**, 236–253.

Sheridan, R. C. 1979 Chemical fertilizers in southern agriculture. *Agricultural History* **53**, 308–318.

Shruthi, R. B. V., Kerle, N. & Jetten, V. 2011 Object-based gully feature extraction using high spatial resolution imagery. *Geomorphology* **134**, 260–268.

Shruthi, R. B. V., Kerle, N., Jetten, V., Abdellah, L. & Machmach, I. 2015 Quantifying temporal changes in gully erosion areas with object oriented analysis. *Catena* **128**, 262–277.

Stocking, M. A. 1980 Examination of the factors controlling gully growth. In: *Assessment of Erosion* (M. de Boodt & D. Gabriels, eds). John Wiley and Sons Ltd, Chichester, UK, pp. 505–520.

Tarolli, P., Arrowsmith, J. R. & Vivoni, E. R. 2009 Understanding earth surface processes from remotely sensed digital terrain models. *Geomorphology* **113**, 1–3.

Tuckfield, C. G. 1964 Gully erosion in the New Forest, Hampshire. *American Journal of Science* **262**, 795–807.

Valentin, C., Poesen, J. & Li, Y. 2005 Gully erosion: impacts, factors and control. *Catena* **63**, 132–153.

Wilkinson, B. H. & McElroy, B. J. 2007 The impact of humans on continental erosion and sedimentation. *GSA Bulletin* **119**, 140–156.

Yang, X., Li, M., Na, J. & Liu, K. 2017 Gully boundary extraction based on multidirectional hill-shading from high-resolution DEMs. *Transactions in GIS* **21**, 1204–1216.

First received 19 April 2019; accepted in revised form 6 August 2019. Available online 3 October 2019